Monteiro, P.M.L. & Hull, C.C. (2007). The effect of videokeratoscope faceplate design on radius of curvature maps. OPHTHALMIC AND PHYSIOLOGICAL OPTICS, 27(1), pp. 76-84. doi: 10.1111/j.1475-1313.2006.00426.x

Title: The Effect of Videokeratoscope Faceplate Design on Radius of Curvature Maps

Authors: P.M.L. Monteiro[1] (E-mail: monteiro@dfisica.ubi.pt)

C.C. Hull[2]

Address: [1] Unidade de Detecção Remota

Universidade da Beira Interior

6200 Covilhã

Portugal

[2] Henry Wellcome Laboratory for Vision Sciences

City University

Northampton Square

London

EC1V 0HB

UK

Abstract

A computer model using finite ray tracing methods was developed to simulate a videokeratoscope analysing an average cornea. Different faceplate designs were tested using five points in the faceplate subtending angles between 15° and 75° in 15° intervals at the corneal vertex. Image quality was assessed by adding the geometrical blurs of the 5 image points. Differences (error) between accurate sagittal radius of curvature and sagittal radius of curvature calculated by the van Saarloos algorithm were calculated for selected surfaces at the same corneal points. The calculations were repeated for the tangential radius of curvature. Differences equal or bigger than 0.02 mm were regarded as clinically significant. The surface that provided the sharpest image for an average cornea was a cylinder with the base 120 mm away from the corneal vertex and a diameter of 26 mm. Changing the faceplate design results in clinically significant differences for an average cornea.

Keywords

Videokeratoscopy; Corneal topography; Faceplate design; Radius of curvature maps

Introduction:

Early keratoscope target designs were flat (Goode (1847) cited in Stone (1994) and Placido (1880)). To provide adequate corneal coverage, a flat target has to be much larger than any other concave target placed at the same distance as has been illustrated by Stone (1962) and Fowler (1994). Ludlam and Wittenberg (1966) report the last use of a flat target by Reynolds and Kratt (1959). Since then it appears that this faceplate geometry has been largely discontinued. Berg (1927), (cited by Ludlam and Wittenberg (1966)), appears to be the first investigator to use a non-flat target when he employed two perpendicular arcs to increase the corneal coverage. Overviews of these early faceplate designs can be found in Ludlam and Wittenberg (1966) and Mammone *et al.* (1990).

Wittenberg and Ludlam (1970) presented results on optimum faceplate designs both for a spherical and elliptical reflecting surface (resembling the cornea). They concluded that an elliptical target was the best design but the theoretical calculations and the experimental work resulted in different ellipsoidal shapes. However, their use of a vertical line target, which is focused sharply in the sagittal focal plane, would not necessarily be expected to agree with calculations that used a formula for tangential focus. This could explain the discrepancy between their theoretical and experimental results. In addition, the large stop size used would introduce other aberrations making the theory only an approximation.

Mandell and St. Helen (1971) determined experimentally the best faceplate design for spherical and parabolic reflecting surfaces using a target with moving parts. No results were presented that attempted to fit a particular surface form to the final result. In addition, neither the spherical nor parabolic surfaces used are a good approximation to the human cornea.

Rowsey (1983) and Binder (1995) claimed that a parabolic faceplate design would decrease optical aberrations allowing for a flat image plane. Although no experimental work was presented to support this claim, it may arise from the fact that the sagittal and tangential image surfaces are parabolic in form for a plane target (Hecht (1998)). Reversing the path of the rays, a parabolic faceplate would result in a flat image surface.

Modern keratoscopes have faceplate designs that often depart from the conic section geometry that has been investigated by earlier workers. In addition, the speed of computer ray tracing now allows us to carry out a more extensive investigation than previously of the optimum faceplate design to achieve best ring mire image quality. The aim of this study is therefore to determine the effect of faceplate geometry on image quality and hence the accuracy of data produced by computer videokeratoscopes. This would allow us to understand the advantages of the plethora of designs that are currently available commercially and to know whether differences in the results produced by corneal topographers with various faceplate geometries may be clinically significant.

Methods:

Determination of best faceplate design

A computer model of a videokeratoscope was developed using Borland C++ Development Suite v5.0 (Borland International Inc, Scotts Valley, CA, USA) and employing finite ray tracing techniques common in computer-aided optical design. The average corneal surface was simulated by a prolate ellipsoid with a 7.72mm central radius of curvature, and a *p*-value of 0.81 (Guillon et al. (1986)) and the surface given by the well known equation

$$x^2 + y^2 = 2Rz - pz^2 . \qquad (1)$$

R is the apical radius of curvature and (*x,y,z*) is a Cartesian coordinate system with origin at the surface vertex and the z-axis aligned with the axis of revolution of the surface (Baker, (1943)). The *p*-value controls the rate of peripheral flattening and hence the conic surface type: $p > 1$ oblate ellipsoid, $p = 1$ sphere, $0 < p < 1$ prolate ellipsoid, $p = 0$ paraboloid and $p < 0$ hyperboloid. Cones, although degenerate, can be modelled as a special case of a conicoid by setting $R = 0$. A negative p-value can then be used to control the aperture angle.

This corneal model was considered reasonable for diameters up to 9mm. In the periphery the surface flattens rapidly towards the limbus and can no longer be

adequately approximated by a conicoid as has been noted by Waring among others (Waring (1989)).

All the modelled faceplate geometries, (plane, conic section, cylinder and cone), had a pupil diameter of 9mm, which is approximately the average aperture in the faceplate seen in several commercial instruments. The models were tested at working distances, *d*, of 120mm, 80mm and 50mm (corneal vertex to the pupil plane of faceplate) (figure 1(b)). These values were again chosen to cover the range used by several commercial instruments.

For the cylindrical design (figure 1(a)), the diameter of the cylinder, ϕ, was changed from 25mm to 240mm in 1mm steps for each of the three working distances. Diameters less than 25mm were not tested because it would be difficult to manufacture such surfaces and diameters larger than 240mm would approximate a plane surface.

Cones were tested at each distance with semi-aperture angles ranging from 1 to 89 degrees in 1-degree steps (*Fig 1b*). The other conical surfaces were modelled by *p-value* and radius of curvature. For each *p-value* the radius of curvature was changed from 5 to 250mm in 5mm steps. A radius of curvature bigger than 250mm would represent almost flat surfaces for the diameter analysed. Negative *p* values, corresponding to a hyperbolic surface, were tested and incremented in such a way that the asymptotic line (figure 2) would change by 1-degree for each increment. A fixed increment to *p* wasn't used in

the hyperbola because it varies non-linearly with the slope of the asymptotic lines.

For ellipsoids ($p > 0$), the *p-value* increment was fixed at 0.1. For each radius of curvature, the last *p*-value tested would be the one corresponding to a surface that didn't intersect a 45 degrees line from the corneal vertex (figure 3).

In order to maximise accuracy the program only processes faceplate shapes such that at least an 8mm corneal diameter is analysed. This is the total coverage claimed by several instrument manufacturers.

Five points in the faceplate subtending 15, 30, 45, 60 and 75 degrees at the corneal apex were initially selected. Cones, cylinders, hyperboloids and paraboloids will always have points that subtend these five angles. Spheres and ellipsoids can only increase in diameter until a certain point, and then start decreasing, so it was not always possible to find the five points.

After determining the position of the tangential plane focus (see appendix) for each of the five points in the faceplate, the range of these focal positions was calculated. The focal plane was then shifted from the tangential focus position closest to the faceplate to the furthest in 1 μm intervals. For each focal plane position the tangential blurs for the five points are summed. The best focal plane position for a given surface, the plane where the sharpest image is

obtained, was considered to be the one that has the smallest value of the total blur.

All faceplate designs that passed the 8 mm minimum corneal coverage criterion were divided in four classes. The first class included the ones that produced minimum blur sum differences $\leq$ 0.001 mm from the best, the second $\leq$ 0.01 mm, the third $\leq$ 0.1 mm and the fourth > 0.1 mm.

Influence of faceplate design on radius of curvature maps

The best faceplate design and a surface representing each of the minimum blur sum based classes, mentioned above, were compared. Since each surface is tested separately and there are only five surface geometries to compare, computation time is no longer a problem, hence the number of points tested in each faceplate was increased. Sixteen points were selected, which is equivalent to eight rings on the faceplate. This number is similar to that used in videokeratoscopes when analysing ring edges. Videokeratoscopes that have a large number of rings do not analyse ring edges but the average position of the complete image ring, since the image is very thin.

Sagittal and tangential radii of curvature were calculated for the simulated cornea by the van Saarloos algorithm (van Saarloos and Constable (1991)) for the best and for a representative of each of the other four minimum blur sum

based classes. These designs were also selected since they are similar to the faceplates used in commercial instruments.

A problem with calculating difference maps for different faceplate shapes (with the same number of rings) is that the reflection points on the simulated cornea will not be the same. To overcome this problem the radial coordinates for the corneal reflection points for the best faceplate surface were used as a reference and the radius of curvature for the same points was calculated for the other faceplate designs. This was done by linear interpolation of radius of curvature between two calculated corneal points. For the selected reference points the sagittal and tangential radius of curvature were calculated from the simulated cornea parameters (apical radius and *p* value). For each faceplate design, the radius of curvature error was calculated for each corneal reference point. This error was determined by subtracting the calculated radius of curvature (in the van Saarloos algorithm) from the actual radius of curvature taken from equations 2 and 3. This process was applied both to the sagittal and tangential radius of curvature values resulting in the sagittal radius error and tangential radius error. These errors were plotted on graphs and compared between faceplates with 9 mm pupils and the image plane at best focus. The experiment was then repeated with the image plane at the first image ring focus.

$$R_s = \sqrt{x^2 + y^2 + (R - pz)^2} \qquad (2)$$

$$R_t = \frac{R_s^3}{R^2} \quad (3)$$

Stone (1962) suggested that an accuracy of 0.02 mm is needed for instruments designed to measure radius of curvature of ophthalmic surfaces. This is due to the fact that contact lenses are manufactured in 0.05 mm steps therefore the accuracy should be approximately half that value. Taking this into account a difference between two radii of curvature equal or larger than 0.02 mm was considered as clinically significant for the scope of this work.

Results

a) Determination of best faceplate design

The least sum of the image blurs from the 5 points in the faceplate will be referred to as the 'minimum sum' for the rest of this discussion. Table 1 summarises the minimum sums for the best design of each of the four geometries tested together with details of the design geometry. Statistics on the number of surfaces that fell within four different amounts of mimumum blur sum were also recorded (table 2).

Two surfaces closely matched the optimum design (a cone of diameter 26mm and working distance of 120mm): the first was another cylinder with the base located at 120mm from the cornea and a diameter of 27mm (1mm bigger than

the best), which can be considered ostensibly the same as the optimum design; the second was the best cone whose design details are given in table 1.

b) Influence of faceplate design in power maps

For each one of the groups listed in Tables 1 & 2 a faceplate design with a minimum blur sum close to each group limit was selected. In addition, the selected designs had to resemble those seen in commercial videokeratoscopes so that we could address the question as to whether differences in faceplate design of current instruments cause significant differences in radius of curvature maps. Specifications of the five surfaces tested are given in table 3.

For simplicity the selected surfaces will be labelled surfaces 1 to 5 respectively. The sagittal radius of curvature errors (*SRE*) and tangential radius of curvature errors (*TRE*) calculated for each one of the five faceplate designs are represented in figures 4 and 5 respectively. These errors were calculated using a 9 mm pupil in the faceplate and for the image plane at best focus. In the abscissas *d* is the distance from the corneal point to the axis of the simulated cornea measured perpendicular to the axis. The markers on the error curves indicate the radial coordinates *d*, for which radii of curvature were calculated for all surfaces.

The sagittal and tangential radius of curvature errors for a 9 mm pupil diameter in the faceplate and image plane at the focus of the first ring mire image are represented in figure 6 and figure 7 respectively.

Discussion

a) Determination of best faceplate design

For the best conoidal and best flat surface, the blur patterns are partially vignetted at the 75 degrees points. This vignetting is an artefact of the program due to the corneal diameter being limited to 9 mm. In the periphery the real cornea adopts a flatter shape and the rays would strike that part without being vignetted. As a result the blur sum would be bigger than actually is measured in the simulation. Within the minimum blur sums (minimum value of the sum of the radial geometrical blurs for five predefined object points) for each type of surface, the flat and conoidal surfaces present the highest values. For these two cases the vignetting is of no concern because it would make the minimum blur sums even larger. The best cone and the best cylinder do not induce vignetting at the 75 degrees points. The minimum blur sums for these two particular surfaces are therefore realistic within the limits of the simulation.

Figure 8 displays the distance of the tangential focus positions from the paraxial plane for 15 ring edges on the best cylinder. From this figure it can be seen why that cylinder produces the minimum blur sum. The first and last set of edges are focused near the paraxial plane (0 mm on the graph) and only the intermediate edges are focused away from the paraxial plane. Hence if the image plane is set for the first ring edge (paraxial plane) the blur sum will be small since only the intermediate rings will be out of focus.

In order to fill the pupil, a bundle of rays reflected on the cornea must spread less if the cornea is further away. This explains why surfaces placed at larger working distances present smaller blur sums. On the other hand the distance has to be limited for an adequate corneal area to be analysed since it was found by experimentation that as the working distance increases the analysed corneal area is reduced.

b) Influence of faceplate design on radius of curvature maps

Analysis of figure 4 shows large sagittal radii errors for all surfaces until ring edge 4. From ring edge 5 only surfaces 4 and 5 present errors outside the ±0.02 mm tolerances. The large central error is due to the defocusing of the central rings, resulting in incorrect ring mire image edge position. Since these curves were calculated for the best focus based on the minimum blur sum, this shifts the focus to the intermediate rings. The central and peripheral rings will be out of focus. However focusing errors for the central mires will have a bigger effect than focusing errors for the more peripheral; the same amount of error will represent a substantial percentage of a smaller ring mire image height and a smaller percentage of a large mire.

Analysis of figure 5 shows large tangential radii errors for all surfaces for central and peripheral rings, while intermediate rings display less error. Central ring errors result from the same causes specified for sagittal error. Peripheral ring

errors are due to the method used by the van Saarloos algorithm to calculate tangential radius of curvature. It considers that three consecutive corneal points share the same centre of curvature to obtain surface smoothness. However in an aspheric surface (with $p<1$) the centre of curvature for peripheral points is different for each points and gets progressively further away from the surface axis. This fact explains the larger error for outer rings.

On figure 6 the image plane was changed from best focus to focus on the inner edge of the first ring mire image. This leads to an accurate edge position resulting in an accurate apical radius calculation for all surfaces. The shift in focus increases the blur for peripheral points. However it doesn't result in a clinically significant error increment when compared to figure 4. This finding suggests that focusing at the first ring mire image inner edge is better than focusing at the best focus position. An interesting effect, magnified by the scale change, is the oscillation of the graphs. It can be explained by the effect of focus on consecutive ring edges. The image of the inner ring edge of an image ring will look smaller when out of focus, while the image of the outer edge will look larger. This results in a decrease and an increase in the calculated radius of curvature respectively.

Figure 7 shows that once again the tangential radius of curvature error is larger than the sagittal radius of curvature error. The error also increases to the peripheral points for the reasons explained earlier. It can also be concluded that the large tangential radius error is not caused by focus but by the algorithm

itself. It is also interesting to note that surface 1 does not seem to be affected by this algorithm error that leads to a tangential radius of curvature error increment for the peripheral rings.

As to the influence of faceplate design on radius of curvature maps, analysis of all data shows that different faceplate designs will lead to clinically significant differences. Although the curves displayed do not show differences directly they represent them, since the radius error for the same point in each curve results from the subtraction of the calculated radius of curvature from the accurate radius of curvature. The accurate radius of curvature for each curve point is the same for all curves at that point.

There is a small degree of approximation in the differences. As previously stated differences were calculated for the same corneal points using surface 1 as a reference. For each surface the sagittal or tangential radius of curvature at the corneal points heights determined for surface 1 were calculated by linear interpolation. When the smallest or highest corneal points in surface 1 are used, one of the bracketing points in other surfaces necessary to the interpolation may be missing. In those cases differences had to be taken at different corneal points, but presented in the graphs as being calculated at the same corneal points. For the available data the contribution of this error for the differences was negligible since the points were very close.

Selecting the measurement point on the cornea to be the same height as the image introduces a small error although it was the approach originally adopted by Rowsey, (1983). Determination of the corneal measurement point has been done in many ways (Mandell & St Helen (1971), Doss *et al.* (1981), Klein (1992) and Halstead *et al.* (1995)) although a full investigation of errors and limitations goes beyond the scope of the current study.

Conclusions

The surface that provides the sharpest image for an average cornea is a cylinder with base 120-mm away from the corneal vertex and a diameter of 26-mm. Ten other designs tested produced a total image blur from five assessed points within 10μm of the best found. Increasing the working distance improves image quality but decreases the analysed corneal area. A balance must be found to provide optimum results.

These results don't show that a cylindrical faceplate provides better results than any other geometry. We can only conclude that this particular cylinder at the specified working distance is the best design. In this section of the work better

results mean that the sums from the blurs of all image points are smaller, which means a sharper image.

Focusing errors have a major effect on radius of curvature errors. Focusing on the image of the first ring edge results in an accurate apical radius and a smaller overall error when compared with best focus.

The method used by the van Saarloos algorithm to calculate the tangential radius of curvature may lead to significant errors for peripheral rings.

We conclude that faceplate geometry can be optimised for image quality and should be considered as an area of design that can be addressed to improve accuracy at a time when keratoscopes are used for measuring corneal aberrations and other parameters relevant to wavefront-guided refractive surgery.

References:

Baker, T.Y. (1943). Ray tracing through non-spherical surfaces. *Proc. Phys. Soc.* **55**, 361-364.

Berg, F. (1927). Undersökningar üver främre hornhinneytans form. *Akad. Afh. Upsala*.

Binder, P.S. (1995) Videokeratography. *CLAO J.* **21**,133-144.

Doss, J.D., Hutson, R.L., Rowsey, J.J., and Brown, D.R. (1981). Method for calculation of corneal profile and power distribution. *Arch. Ophthalmol.* **99**,1261-1265.

Fowler, C.W. and Dave, T.N. (1994). Review of past and present techniques of measuring corneal topography. *Ophthal. Physiol. Optics* **14**, 49-58.

Guillon, M., Lydon, D.P. and Wilson, C. (1986). Corneal topography: a clinical model. *Ophthalm. Physiol. Opt.* **6**, 47-56.

Halstead, M.A., Barsky, B.A., Klein, S.A., and Mandell, R.B. (1995). A spline surface algorithm for reconstruction of corneal topography from a videokeratographic reflection pattern. *Optom. Vis. Sci.* **72**, 821-827.

Hecht, E. (1998). *Optics*. 3rd Edition, Addison-Wesley, MA, USA pp. 267-268.

Klein, S.A. (1992). A corneal topography algorithm that produces continuous curvature. *Optom. Vis. Sci.* **69**, 829-834.

Longhurst, R.S. (1973). *Geometrical and Physical Optics*. 3rd Edition, Longman Scientific and Technical, England, pp. 406-407.

Lotmar, W. (1971). Theoretical eye model with aspherics. *J. Opt. Soc. Am.* **61**, 1522-1529.

Ludlam, W.M. and Wittenberg, S. (1966). Measurement of the ocular dioptric elements utilizing photographic methods, Part II Cornea - Theoretical considerations. *Am. J. Optom.* **43**, 249-267.

Mammone, R.J., Gersten, M., Gormley, D.J., Koplin, R.S., and Lubkin, V.L. (1990). 3-D Corneal modeling system. *IEEE Trans. Biomed. Eng.* **37**, 66-72.

Mandell, R.B. and St.Helen, R. (1971). Mathematical model of the corneal contour. *Br. J. Physiol. Optics* **26**, 183-197.

Mandell, R.B. (1992). The enigma of the corneal contour. *CLAO J.* **18**, 267-272.

Plácido, A. (1880). Novo instrumento para análise imediata das irregularidades de curvatura da córnea, *Periódico de Oftalmologia Prática* **2**,44-49.

Reynolds, A.E. and Kratt, H.J. (1959). The photo-electronic keratoscope. Contacto **3**, 53-59.

Roberts, C. (1994). Characterization of the inherent error in a spherically-biased corneal topography system in mapping a radially aspheric surface. *J. Refract. Corneal Surg.* **10**, 103-116.

Roberts, C. (1994b). The accuracy of 'power' maps to display curvature data in corneal topography systems. *Invest. Ophthalmol. Vis. Sci.* **35**, 3525-3532.

Rowsey, J.J ; Isaac, M.S (1983). Corneoscopy in keratorefractive surgery. *Cornea* **2**, 133-142.

Smith, W.J. (1966). *Modern Optical Engineering*. McGraw-Hill, NY, USA p. 393.

Stone, J. (1962). The validity of some existing methods of measuring corneal contour compared with suggested new methods. *Br. J. Physiol. Optics* **19**, 205-230.

Stone, J. (1994). Keratometry and Specialist Optical Instrumentation. In: *Contact Lens Practice.* (eds Ruben, M. and Guillon, M.), Chapman and Hall, London UK pp. 284-285.

van Saarloos, P.P. and Constable, I.J. (1991). Improved method for calculation of corneal topography for any photokeratoscope geometry. *Optometry And Vision Science* **68**, 960-965.

Waring III, G.O. (1989). Making sense of keratospeak II: Proposed conventional terminology for corneal topography. *Refractive & Corneal Surgery* **5**, 362-367.

Wittenberg, S. and Ludlam, W.M. (1970). Planar reflected imagery in photokeratoscopy. *J. Opt. Soc. Am.* **60**, 981-985.

APPENDIX

Tangential focal position determination

The position of the tangential focal line for each point is determined by the intersection of the upper and lower tangential rim rays (figure 9b). This method provides a fast way of finding the tangential focus, which will correspond to the smallest blur of the rings.

Figure 9 shows the image of a point at a 15-degrees angle from the corneal vertex. The point lies in the upper vertical hemi-meridian of a spherical faceplate with 250mm radius of curvature. The pupil size in the faceplate is 9mm located 80mm from the corneal vertex. The image is shown at the best focus position (*b*), 2-μm before (*a*) and 2-μm after (*c*). The intersections of the upper and lower rim rays with the focal plane are represented by *u* and *l* respectively. The tangential blur is the blur dimension in the tangential plane direction, vertical in this particular case.

In the best tangential focus the blur pattern is limited by the upper and lower rim rays in one extremity and by the chief ray in the other (figure 9b). When the focal position is far away from the best focus in both directions, a large blur will occur being limited by the upper and lower rim rays. In the interval between these focal positions and before reaching the best focus in both directions, only one extremity of the blur will be limited by the upper rim ray or lower rim ray. In

this case the only way to predict the other extremity is to trace rays in the tangential plane. The accuracy will be limited by the number of rays traced.

Determination of a ring mire image edge

Geometrical ray tracing allows us to model the irradiance in the image by using the ray density and converting this to a gray-scale representation (figure 10). It can be seen that at the tangential focal plane the edge is sharp. Most edge detection algorithms compute the slope of the edge and estimate the edge by the mid-point of the slope. We have taken the point of half the maximum irradiance as the location of the edge. It should be noted that to accurately model the ring mire image, this geometrical point spread function needs to be convolved with a ring with the result that irradiance values inside the position of peak irradiance shown in the graph (figure 10) will not fall away as indicated.

Table 1 - Minimum blur sums for the best in each of the four categories of faceplate design tested.

Design	**Design Specification**	**Minimum Sum (μm)**
Flat	Working distance 80mm	102.68
Cone	Working distance 120mm Total aperture angle 8^{o}	29.05
Cylinder	Diameter 26mm Working distance 120mm	28.21
Conicoid	Radius of curvature 20mm *p = -0.163* (hyperboloid) Working distance 120mm	55.65

Table 2 – Frequency table for faceplate designs with differences, Δ, from the best minimum sum.

	Δ within 1μm	1 μm - 10 μm	10 - 100 μm	>100 μm
Flat	0	0	1	1
Cone	1	1	120	70
Cylinder	2	7	350	191
Conicoid	0	0	5785	6529

Table 3 – Specifications for the five faceplate designs tested for clinically significant differences in power maps.

Nº	Faceplate type	Design details	Minimum blur (μm)
1	Cylinder	Diameter 26mm, 120mm length	28.21
2	Cone	8^{o} total aperture, 25 mm maximum diameter, 119 mm length	29.05
3	Cylinder	34mm diameter, 119 mm length	37.40
4	Cylinder	49mm diameter, 49 mm length	126.96
5	Cone	160 degree total aperture, 240 mm maximum diameter, 49 mm length	182.99

Figure 1 - Sections of cylindrical and cone shaped faceplates. ***a)*** The angle θ from the cylinder base to the opposite corner can be used to control the diameter ϕ and the length *d*. ***b)*** Cones with semi-aperture angles θ_1 and θ_2. Both cones start at a 9mm pupil aperture.

Figure 2 - Hyperboles with the same apical radius of curvature and asymptotic lines at 30 and 45 degrees inclination. The curves are similar to a cone in the periphery, but different at the centre.

Figure 3 - In a cone-type faceplate it is always possible to define the five points as long as the cone has sufficient length to either side. The same applies to cylindrical, hyperbolic and parabolic faceplates. In spherical and ellipsoidal faceplates the surface can only increase in diameter until a certain point, after which it starts to close. In these cases it is not always possible to find the five points. The figure represents a case in that is only possible to define two of the five points.

Figure 4 - Differences (*SRE*) between accurate sagittal radii of curvature and sagittal radii of curvature calculated by the van Saarloos algorithm for surfaces 1 to 5. Faceplate pupil with 9 mm diameter and image plane at best focus.

Figure 5 - Differences (*TRE*) between accurate tangential radii of curvature and tangential radii of curvature calculated by the van Saarloos algorithm for surfaces 1 to 5. Faceplate pupil with 9 mm diameter and image plane at best focus.

Figure 6 - Differences (*SRE*) between accurate sagittal radii of curvature and sagittal radii of curvature calculated by the van Saarloos algorithm for surfaces 1 to 5. Faceplate pupil with 9 mm diameter and image plane at first ring mire image focus.

Figure 7 - Differences (*TRE*) between accurate tangential radii of curvature and tangential radii of curvature calculated by the van Saarloos algorithm for surfaces 1 to 5. Faceplate pupil with 9 mm diameter and image plane at first ring mire image focus.

Figure 8 - Tangential focus position, measured from the paraxial plane (located at 0 mm mark), for 15 ring edges on the best cylinder.

Figure 9 – Image of an object point near the instrument axis for slightly different positions of the image plane. Tangential blurs in cases *a)*, *b)* and *c)* are 1.262, 1.152 and 1.248 μm respectively. The image plane position corresponding to the intersection of upper and lower rim rays (*b*) is the best focus. The dimensions presented are small but object points near the instrument axis illustrate the principle better. The same principle applies to object points further off axis.

Figure 10 - Image point corresponding to a ring mire edge subtending 15º from the corneal vertex in the best surface, and respective estimated irradiance pattern in the tangential plane. The ring edge was considered to be positioned where the irradiance is half the maximum value for that object point.

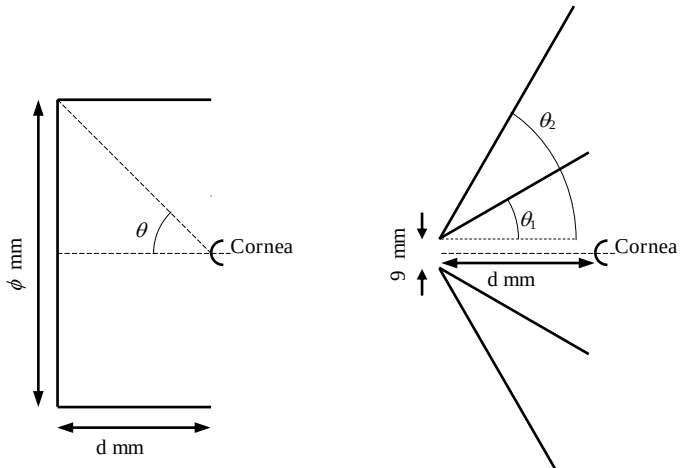

a) **b)**

Fig1

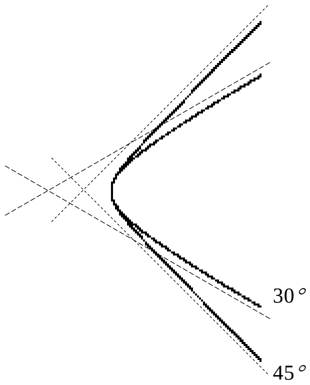

Fig2

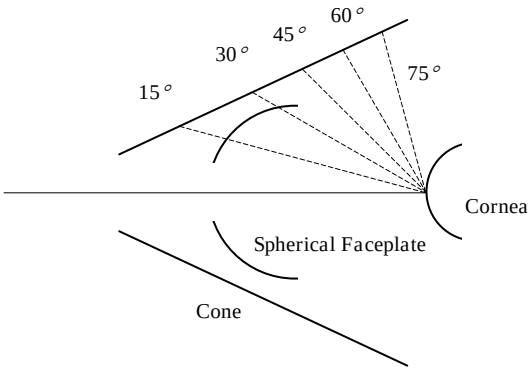

Fig 3

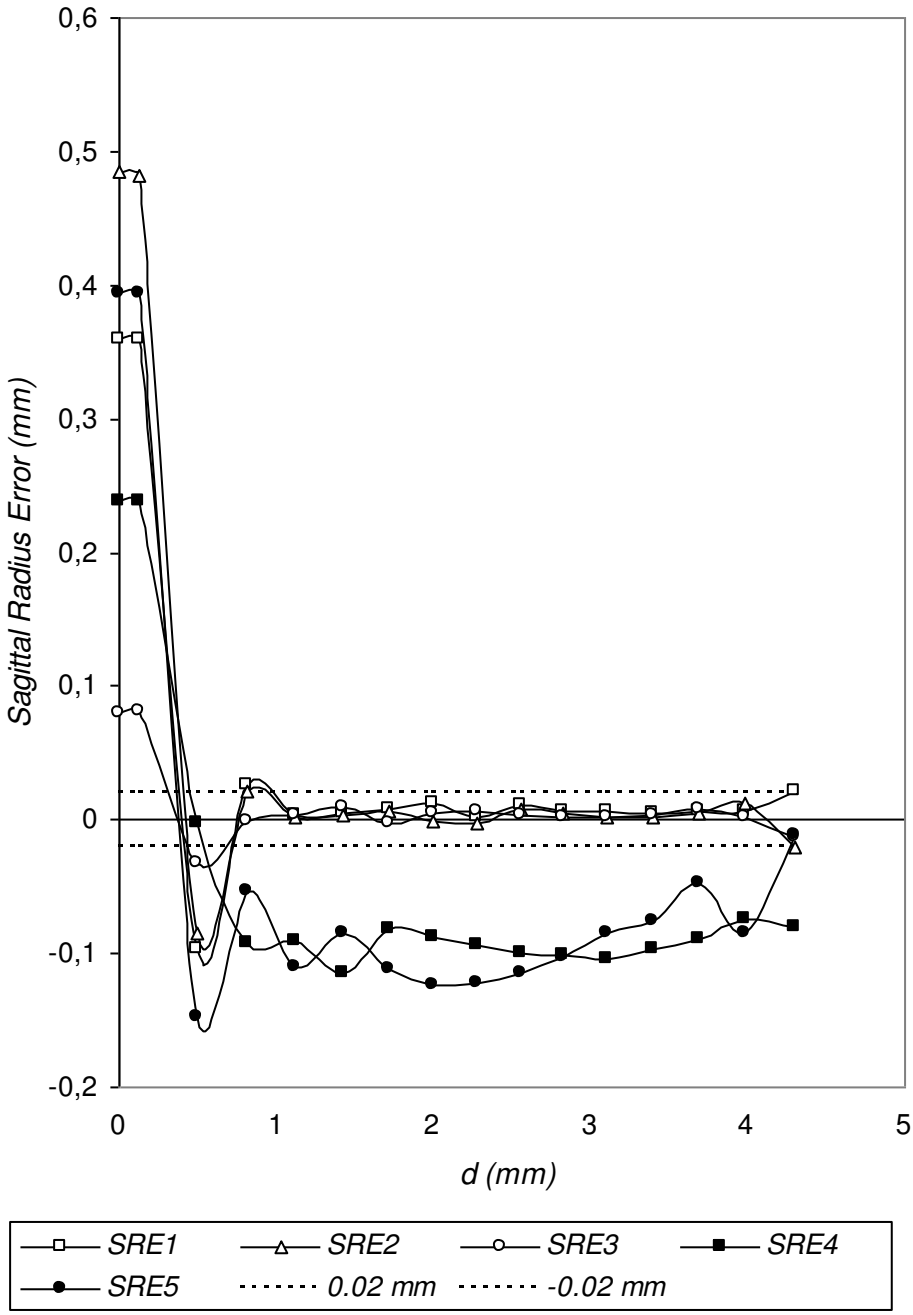
0,6
0,5
0,4
0,3
0,2
0,1
0
-0,1
-0,2
Sagittal Radius Error (mm)
0
1
2
3
4
5
d (mm)
SRE1
SRE2
SRE3
SRE4
SRE5
0.02 mm
-0.02 mm

Fig. 4

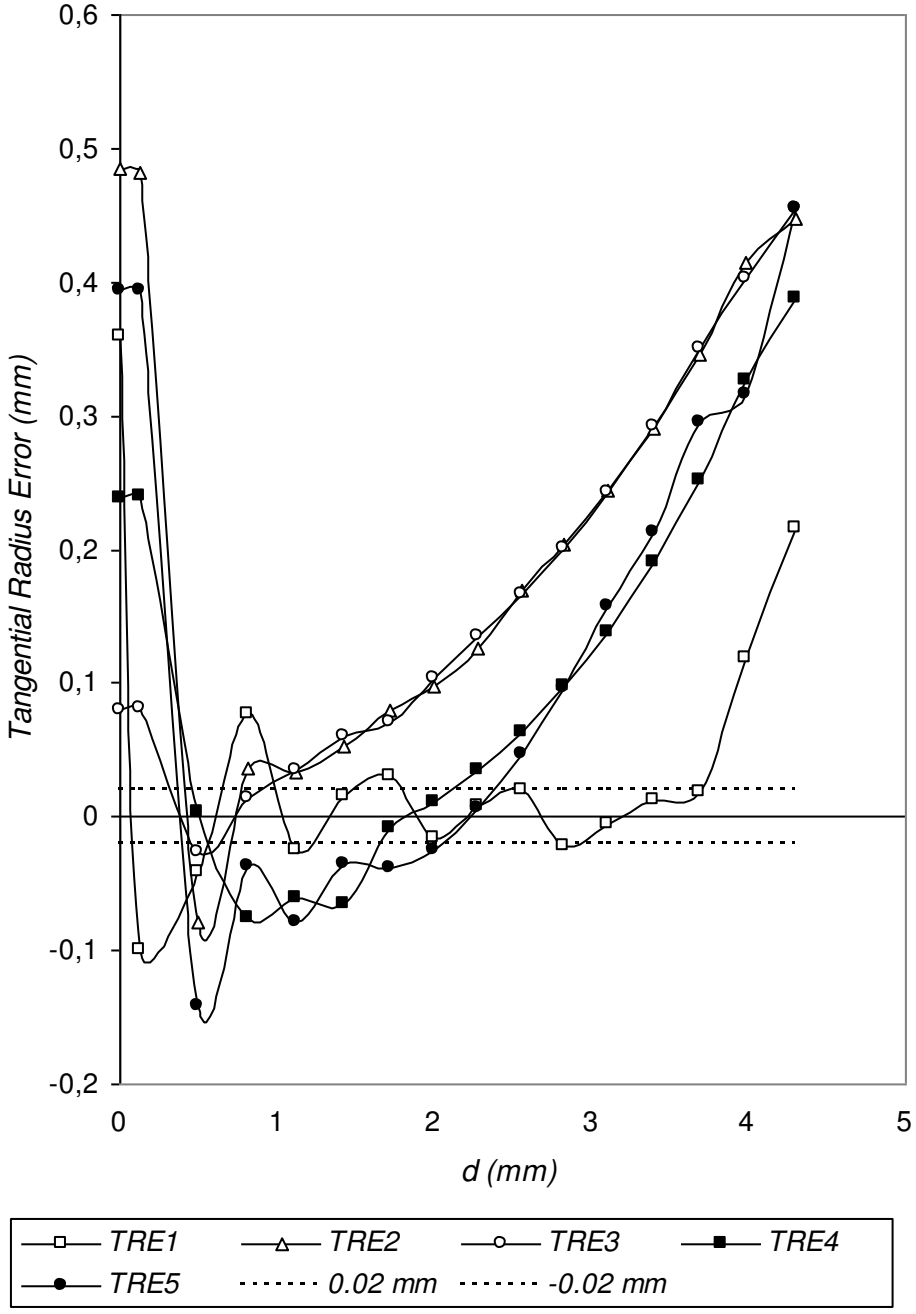
0,6
0,5
0,4
0,3
0,2
0,1
0
-0,1
-0,2
Tangential Radius Error (mm)
0
1
2
3
4
5
d (mm)
TRE1
TRE2
TRE3
TRE4
TRE5
0.02 mm
-0.02 mm

Fig. 5

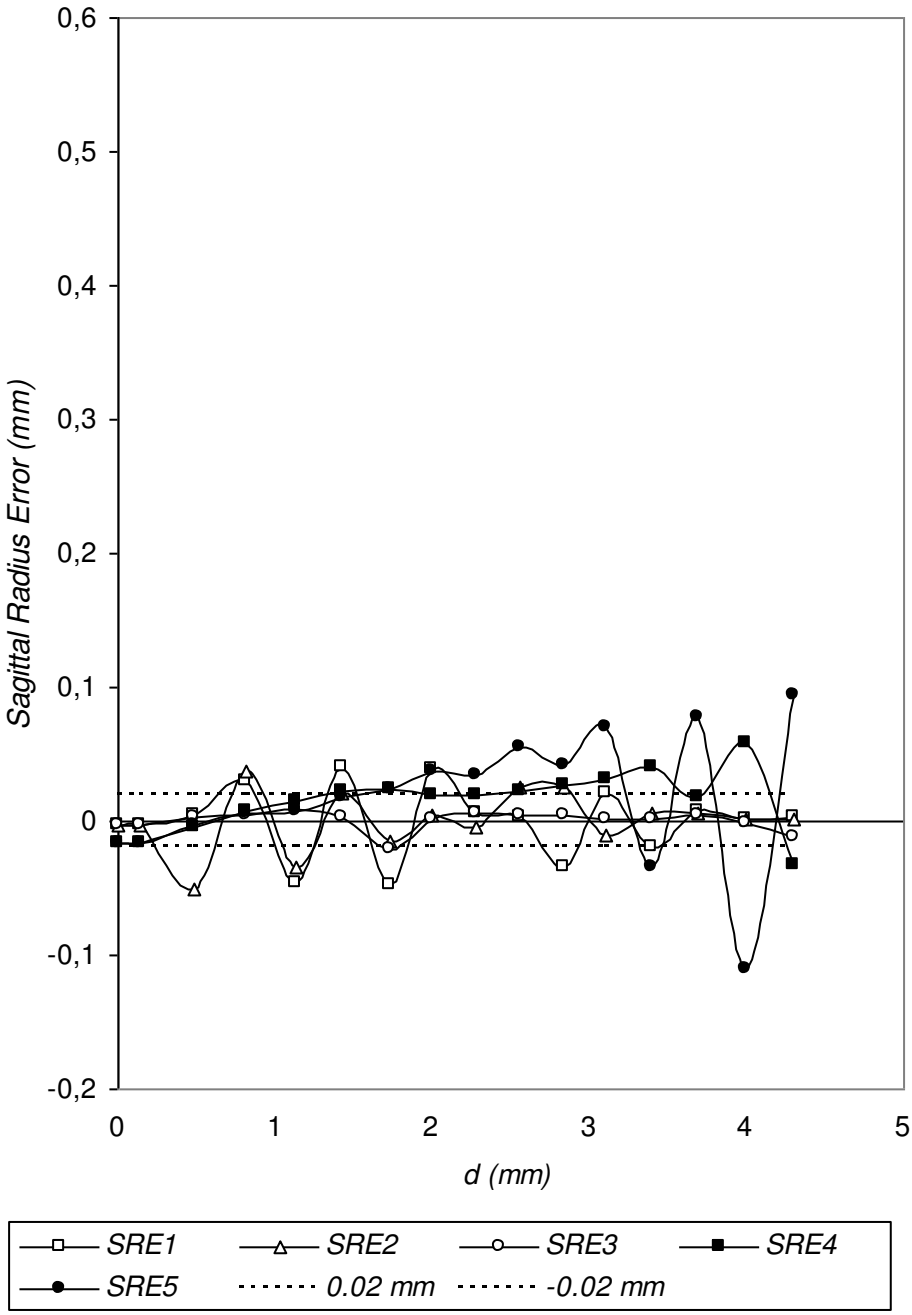
0,6
0,5
0,4
0,3
0,2
0,1
0
-0,1
-0,2
Sagittal Radius Error (mm)
0
1
2
3
4
5
d (mm)
SRE1
SRE2
SRE3
SRE4
SRE5
0.02 mm
-0.02 mm

Fig. 6

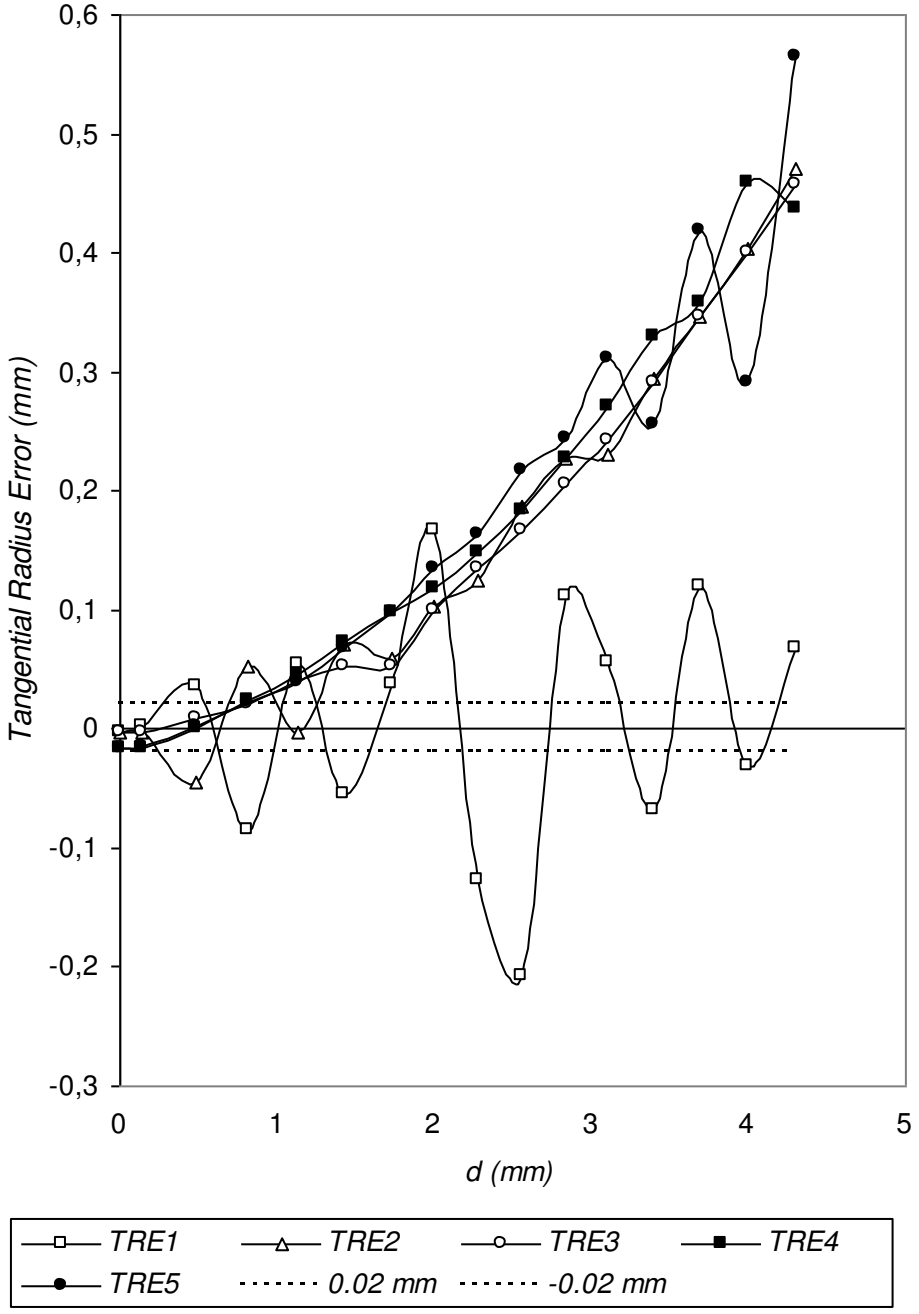
0,6
0,5
0,4
0,3
0,2
0,1
0
-0,1
-0,2
-0,3
Tangential Radius Error (mm)
0
1
2
3
4
5
d (mm)
TRE1
TRE2
TRE3
TRE4
TRE5
0.02 mm
-0.02 mm

Fig. 7

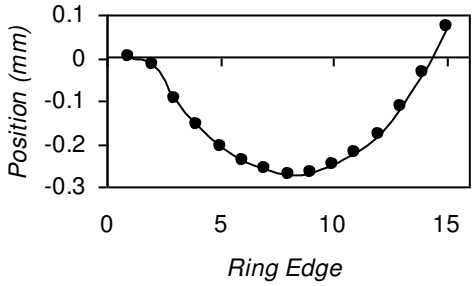

Fig. 8

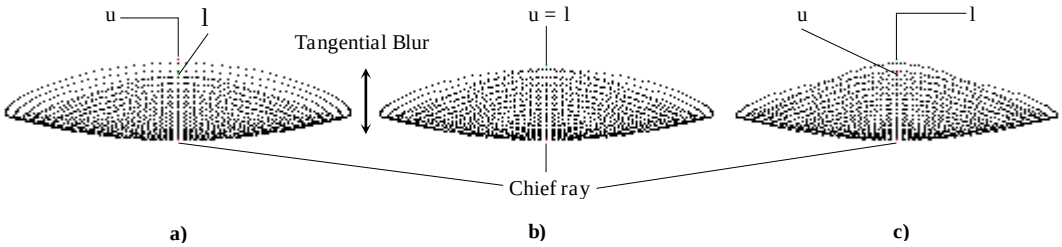

Fig. 9

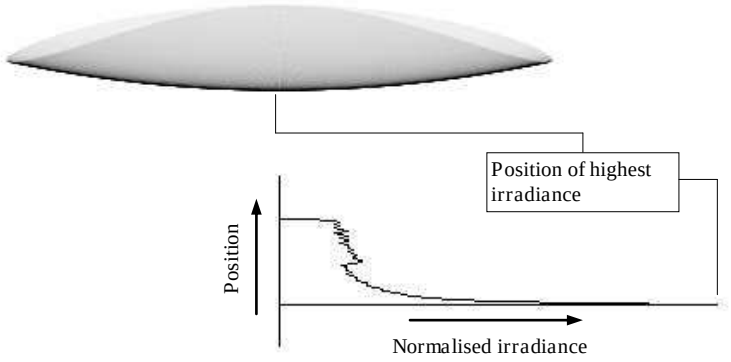
Position of highest irradiance
Position
Normalised irradiance

Fig. 10